Title

Tau PET imaging with 18F-PI-2620 in aging and neurodegenerative diseases

Journal

European Journal of Nuclear Medicine and Molecular Imaging, 48(7)

ISSN

1619-7070

Authors

Mormino, Elizabeth C
Toueg, Tyler N
Azevedo, Carmen
et al.

Publication Date

2021-07-01

DOI

10.1007/s00259-020-04923-7

Peer reviewed

European Journal of Nuclear Medicine and Molecular Imaging
https://doi.org/10.1007/s00259-020-04923-7

ORIGINAL ARTICLE

Tau PET imaging with ^{18}F-PI-2620 in aging and neurodegenerative diseases

Elizabeth C. Mormino[1] · Tyler N. Toueg[1] · Carmen Azevedo[2] · Jessica B. Castillo[2] · Wanjia Guo[3] · Ayesha Nadiadwala[1] · Nicole K. Corso[1] · Jacob N. Hall[1] · Audrey Fan[2] · Alexandra N. Trelle[3] · Marc B. Harrison[3] · Madison P. Hunt[3] · Sharon J. Sha[1] · Gayle Deutsch[1] · Michelle James[1,2] · Carolyn A. Fredericks[1] · Mary Ellen Koran[2] · Michael Zeineh[2] · Kathleen Poston[1] · Michael D. Greicius[1] · Mehdi Khalighi[2] · Guido A. Davidzon[2] · Bin Shen[2] · Greg Zaharchuk[2] · Anthony D. Wagner[3] · Frederick T. Chin[2]

Received: 1 December 2019 / Accepted: 9 June 2020

Abstract

Purpose In vivo measurement of the spatial distribution of neurofibrillary tangle pathology is critical for early diagnosis and disease monitoring of Alzheimer's disease (AD).

Methods Forty-nine participants were scanned with ^{18}F-PI-2620 PET to examine the distribution of this novel PET ligand throughout the course of AD: 36 older healthy controls (HC) (age range 61 to 86), 11 beta-amyloid+ (Aβ+) participants with cognitive impairment (CI; clinical diagnosis of either mild cognitive impairment or AD dementia, age range 57 to 86), and 2 participants with semantic variant primary progressive aphasia (svPPA, age 66 and 78). Group differences in brain regions relevant in AD (medial temporal lobe, posterior cingulate cortex, and lateral parietal cortex) were examined using standardized uptake value ratios (SUVRs) normalized to the inferior gray matter of the cerebellum.

Results SUVRs in target regions were relatively stable 60 to 90 min post-injection, with the exception of very high binders who continued to show increases over time. Robust elevations in ^{18}F-PI-2620 were observed between HC and Aβ+ CI across all AD regions. Within the HC group, older age was associated with subtle elevations in target regions. Mildly elevated focal uptake was observed in the anterior temporal pole in one svPPA patient.

Conclusion Preliminary results suggest strong differences in the medial temporal lobe and cortical regions known to be impacted in AD using ^{18}F-PI-2620 in patients along the AD trajectory. This work confirms that ^{18}F-PI-2620 holds promise as a tool to visualize tau aggregations in AD.

Keywords Alzheimer's disease · Human aging · Tau PET · Neurofibrillary tangles

Background

Aggregations of beta-amyloid (Aβ) into extracellular plaques and hyperphosphorylated tau into intracellular neurofibrillary tangles are the hallmark pathological features of Alzheimer's disease (AD) [1]. The ability to assess Aβ plaques in vivo with positron emission tomography (PET) has been available for over a decade, whereas tau PET ligands have become available only recently. ^{18}F-Flortaucipir (previously known as ^{18}F-T807 and ^{18}F-AV-1451) was the first promising tau PET ligand with initial publications beginning in 2013 [2], with recent work showing correspondence between in vivo imaging and postmortem tau aggregations within the same participants [3]. In a short time period, this ligand has been applied widely in research studies, showing robust group

This article is part of the Topical Collection on Neurology

Electronic supplementary material The online version of this article (https://doi.org/10.1007/s00259-020-04923-7) contains supplementary material, which is available to authorized users.

✉ Elizabeth C. Mormino
bmormino@stanford.edu

[1] Department of Neurology and Neurological Sciences, Stanford Medical School, 300 Pasteur Drive, Stanford, CA 94305, USA

[2] Department of Radiology, Stanford Medical School, Stanford, CA, USA

[3] Department of Psychology, Stanford University, Stanford, CA, USA

Published online: 23 June 2020

differences between older healthy controls and cognitively impaired patients with mild cognitive impairment (MCI) and AD dementia [4, 5], early signal among older healthy controls (HC) that predicts future memory decline [6–8], and spatial patterns of uptake that align with brain networks selectively impaired in atypical clinical presentations of AD [9].

The ability to measure tau aggregation accurately holds particular promise as a biomarker for AD, given that tau deposits are known to be proximal to clinical deficits [10], and the majority of Aβ-induced toxicity is thought to be mediated by tau accumulation [11]. There are currently a handful of promising tau PET ligands under investigation. Although initial work with tau PET has provided important insights into the potential of this tool to improve our understanding of AD and provide a means to assess disease modifying therapies, a number of uncertainties remain such as the degree to which off-target signal contaminates target signal across various tau PET ligands. We therefore applied the novel tau PET tracer ^{18}F-PI-2620 [12, 13] across the spectrum of AD and in older healthy controls. ^{18}F-PI-2620 has shown initial promise in detecting tau aggregates in patients with AD [12, 14, 15], as well as high selectivity for 3R/4R tau aggregates [13]. The overall goal was to provide a comprehensive overview of the spatial pattern and magnitude of signal with this novel tau ligand in regions relevant to AD.

Methods

Participants

Forty-nine participants were recruited into this study and underwent a ^{18}F-PI-2620 tau PET-MR scan. Older normal controls were recruited through an ongoing study of normal aging, the Stanford Aging and Memory Study (SAMS). SAMS is an NIH-funded imaging-biofluid observational cohort study of normal aging that began enrolling in 2014 (age 60+). All HC recruited through SAMS were classified as clinically normal at a clinical consensus meeting by a panel of neurologists and neuropsychologists. Patients with cognitive impairment (CI; either a clinical diagnosis of MCI or AD dementia) and semantic variant primary progressive aphasia (svPPA) were recruited through the Stanford Alzheimer's Disease Research Center (ADRC) or the Stanford Center for Memory Disorders. All CI patients diagnosed clinically with MCI or AD dementia were confirmed to have biomarker evidence of AD using pre-existing cerebrospinal fluid (CSF) or amyloid PET data. To assess global cognition, Mini-Mental State Examination (MMSE) was available for all HC, whereas the Montreal Cognitive Assessment (MoCA) was available for all patients with MCI or AD dementia (with the exception of one atypical AD case who was too impaired to complete the MoCA and a MCI case that had MMSE instead of the MoCA).

The study protocol was approved by the Stanford Institutional Review Board and the study was conducted in accordance with the Declaration of Helsinki. All participants (or their legal representatives) provided written informed consent.

Data acquisition

^{18}F-PI-2620 was synthesized at the Stanford Cyclotron facility at the Richard M. Lucas Center for Imaging using a previously published protocol [13]. Precursor was provided by Life Molecular Imaging to make ^{18}F-PI-2620. In brief, ^{18}F-PI-2620 was prepared via a two-step synthetic route including radiofluorination and hydrolysis using an automated radiosynthesis platform (GE TRACERlab FX N). PI-2620 precursor solution (2.0 mg in 0.8 mL anhydrous DMSO) was added into azeotropically dried ^{18}F/K_{222}/K_2CO_3 complex, heated to 150 °C for 15 min, and the crude product was purified on semi-preparative high-performance liquid chromatography (HPLC). The ^{18}F-PI-2620 fraction was formulated in 0.9% sodium chloride injection (USP) containing no more than 10% ethanol and 10 mg of ascorbic acid. ^{18}F-PI-2620 was obtained with 9.62 ± 3.27% radiochemical yield (decay-corrected), 99% radiochemical purity, and molar activity of 138.95 ± 68.20 GBq μmol^{-1}. The range of injected activities was 173.54 to 354.02 MBq, and the average injected activity was 204.65 ± 41.80 MBq. The broad range of injected doses reflects a study protocol change (the study began with an injection of 300 MBq, but was decreased to 185 MBq after further data showed that high image quality was maintained with a lower injection of 185 MBq).

PET scanning was completed at the Richard M. Lucas Center for Imaging, using a simultaneous time-of-flight (TOF)–enabled PET/MRI scanner (Signa 3 T, GE Healthcare), with high sensitivity (23.3 cps/kBq^1). Following a 5 to 10 mCi injection of ^{18}F-PI-2620 into an antecubital vein, all subjects had data collected 60 to 90 min post-injection, and 39 of 49 participants had emission data collected at injection (with a break between 30 and 50 min post-injection). The 10 subjects missing early dynamic data were all healthy control participants.

PET images were reconstructed using TOF optimized subset expectation maximization (TOF-OSEM) with 3 iterations, 28 subsets, and 2.78 × 1.17 × 1.17 mm voxel size. Corrections were applied for detector deadtime, scatter, randoms, detector normalization, and radioisotope decay. Attenuation correction was performed with zero-TE (ZTE) MR imaging for MR attenuation correction (MRAC), which allows direct visualization of bone within the head [16]. PET data were reconstructed into the following frames: 15-s frames for 0 to 5 min post-injection, 1-min frames for 5 to 20 min, and then 5-min frames

for 30 to 100 min post-injection. Standardized uptake values (SUVs) were computed by normalizing to participant weight and injected dose.

Image processing

PET image processing was performed using FSL (https://fsl.fmrib.ox.ac.uk/fsl/fslwiki). Specifically, PET frames were realigned with FSL's FLIRT, using the 5-min PET frame closest to the acquisition of the high-resolution T1 SPGR as the reference frame (ensuring optimal coregistration between PET and the simultaneously collected structural MRI data). We focused on summed data corresponding to 60 to 90 min post-injection, but first examined SUVR values extracted from individual frames as a function of post-injection time. We examined regions of interest known to be impacted in the course of AD according to Braak staging as well as work with other tau PET tracers, which corresponds to the medial temporal lobe (an average across the entorhinal, hippocampus, and amygdala), posterior cingulate cortex, and lateral parietal cortex [4, 17]. Voxelwise SUVR data was examined across diagnostic groups at both the group level and also at the individual participant level to enable exploration of patterns of uptake. Group-level maps were created by spatially normalizing each participant's structural MRI scan to the MNI template [18] using a non-linear transformation (FSL FNIRT), and then applying those transformation parameters to the corresponding voxelwise SUVR PET data. Spatially normalized PET data were then averaged within diagnostic group. For examination of individual-level voxelwise SUVR PET data, images were displayed in each participant's native space.

Structural MRI processing

MRI data was collected simultaneously with the PET data. In the current analysis, we used a high-resolution T1-weighted spoiled gradient recalled echo (SPGR) scan (TR/TE/TI = 7.664/3.09/400 ms, flip angle = 11, 1.2 × 1.1 × 1.1 mm) to define regions of interest (ROI) in each participant's native space using the FreeSurfer software packages [19], version 6.0 (http://surfer.nmr.mgh.harvard.edu/). In brief, structural images were bias field–corrected, intensity-normalized, and skull-stripped using a watershed algorithm. These images underwent a white matter–based segmentation, gray/white matter and pial surfaces were defined, and topology correction was applied to these reconstructed surfaces. Subcortical and cortical ROIs spanning the entire brain were defined in each subject's native space. A single trained operator (TT) visually confirmed resulting surface output and made manual edits and/or added control points when ROI mis-labeling occurred. A bilateral gray matter cerebellum ROI from the subcortical aseg FreeSurfer atlas [20] was extracted for each participant and edited manually to remove the superior portion, given known issues with off-target binding in this region (Supplemental Fig. 1). The gray matter inferior cerebellum ROI was used as a reference region by normalizing the summed PET data by the mean value in this region. We focused on three bilateral target ROIs from the resulting aseg and aparc atlases [20, 21] defined on each subject's FreeSurfer-processed MRI data: medial temporal lobe (combining entorhinal, hippocampus, and amygdala ROIs), posterior cingulate (isthmus cingulate and posterior cingulate), and lateral parietal cortex (inferior parietal, superior parietal, and supramarginal).

Statistical analysis

Demographic group differences were examined using Spearman's rank correlation coefficients for continuous variables and Wilcoxon signed-rank tests for categorical variables. Diagnostic differences for regional SUVRs were determined with non-parametric Wilcoxon signed-rank tests, using the contrast of HC versus CI (MCI and AD dementia). Associations between age and regional SUVRs with the HC group were assessed using Spearman's rank correlation coefficients.

Results

Participants

Participant characteristics are shown in Table 1. There were no significant differences in age between the HC and CI groups ($p = 0.87$). Three of six AD dementia patients and one of five MCI had atypical clinical presentations consistent with posterior cortical atrophy ($N = 4$), whereas the remaining seven patients with cognitive impairment had amnestic presentations [22]. Given known differences in tau binding magnitude and spatial distribution between amnestic and non-amnestic presentations of AD [9], subsequent analyses displayed the four atypical CI patients separately.

Stability across post-injection window

SUVs during the late acquisition period were low in the inferior cerebellum (Fig. 1(A)), did not significantly differ across the HC and CI groups when examining 60–90 min post-injection (Fig. 1(B); $W = 253$, $p = 0.17$), and did not show significant correlations with age within the HC group (Fig. 1(C); rho = 0.02, $p = 0.90$). This pattern suggests this region may be a suitable reference region for simplified semi-quantitative analysis of ^{18}F-PI-2620 and was used to derive SUVRs.

Mean values for AD-relevant target regions in bilateral MTL, posterior cingulate, and lateral parietal cortex were extracted and divided by the mean signal within the inferior cerebellum to derive SUVRs for each frame within each participant. Given that many participants had PET data that

Table 1 Mean and SD are listed for age for HC and CI groups; individual ages for svPPA are listed. All participants had dynamic data collected beginning at injection with the exception of 10 HC individuals. SD=Standard Deviation; HC=Healthy Control; CI=Cognitive Impairment; svPPA=Semantic Variant Primary Progressive Aphasia

	Healthy control	Cognitively impaired	Atypical cognitively impaired	svPPA
N	36	7	4	2
Age	70.5 (6.0)	73.2 (9.2)	65.4 (8.7)	66, 78
Sex (F)	16	4	4	1

extended before 60 min and/or after 90 min post-injection, all available data were plotted to enable visualization over SUVRs over time across all participants (Fig. 2). SUVRs corresponding to the late acquisition were consistently elevated in the MTL in the CI group compared with the majority of HC participants. Further, four HC participants showed SUVR values in the MTL that were consistent with values observed in the CI group. Cortical regions showed more heterogeneity within the CI group, with only some of these participants showing elevated signal in the posterior cingulate and lateral parietal cortex. Conversely, all four atypical CI participants showed robust uptake in these cortical regions. In general, elevations in SUVR were stable between 60 and 90 min post-injection, with the exception of two atypical CI participants with very high binding.

A notable distinction across regions is the range of SUVR values (Fig. 2). In particular, SUVRs from the MTL showed the most restricted range, with maximal values in CI participants around 2.5 and some early elevated signal within a subset of HC participants. In contrast, mean SUVR values greater than 3.5 were present in the posterior cingulate and SUVR values greater than 5 were present in the lateral parietal cortex for two atypical CI participants. Further, SUVRs that exceeded 3 continued to show elevations at higher post-injection windows. Relatively stable SUVRs were observed for moderate binders (SUVR < 3) during the examined time window across the MTL and cortical ROIs.

Differences across the AD spectrum

Voxelwise SUVR maps corresponding to 60 to 90 min post-injection were created and averaged within diagnostic group to enable qualitative examination of the pattern of ^{18}F-PI-2620 uptake. These average maps showed little uptake in HC, other than off-target binding in the retina, substantia nigra, and venous sinuses (Fig. 3(A)). Elevations were observed in the MTL and across multiple cortical association areas in the amnestic CI group (Fig. 3(B)), and robust elevations were present throughout posterior association cortices in atypical AD (Fig. 3(C)).

The ROI analysis revealed significantly elevated SUVRs in the CI group compared with the HC group for MTL ($W = 18$, $p < 0.0001$), posterior cingulate ($W = 55$, $p = 0.00014$), and lateral parietal ($W = 33$, $p < 0.0001$; Fig. 4). This elevation remained significant across all regions after removing the four atypical CI participants (MTL: $W = 9$, $p < 0.0001$; posterior cingulate: $W = 55$, $p = 0.018$; lateral parietal: $W = 33$, $p = 0.0012$). Within the HC group, age was positively associated with SUVRs across all ROIs (MTL: rho = 0.43, $p = 0.0089$; posterior cingulate: rho = 0.37, $p = 0.028$; lateral parietal: rho = 0.40, $p = 0.016$).

Voxelwise SUVR data corresponding to 60 to 90 min post-injection for individual participants are shown for a subset of individual HC (Fig. 5). Consistent with the group-level average (Fig. 3(A)), there was generally low uptake across HC participants, with some evidence of early medial temporal signal in a subset of cases, and off-target binding in the retina,

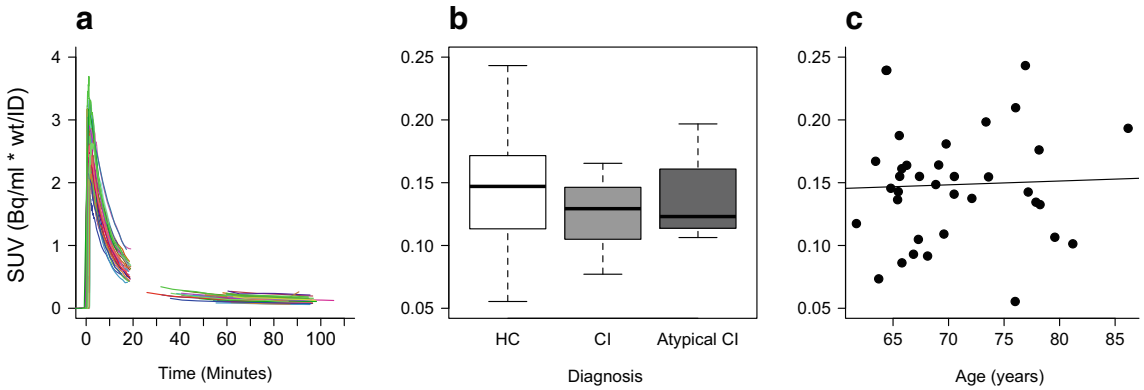

Fig. 1 Inferior cerebellum reference region SUV. Time activity curves showing the mean SUV from the inferior cerebellum reference region across participants (A). SUVs corresponding to 60 to 90 min post-injection by diagnosis (B) as well as by age within the HC group (C). SUV = Standardized Uptake Value; HC = Healthy Control; CI = Cognitive Impairment; Atypical CI = Atypical Cognitive Impairment; Bq/ml = Becquerel/Milliliter; wt/ID = weight/injected dose

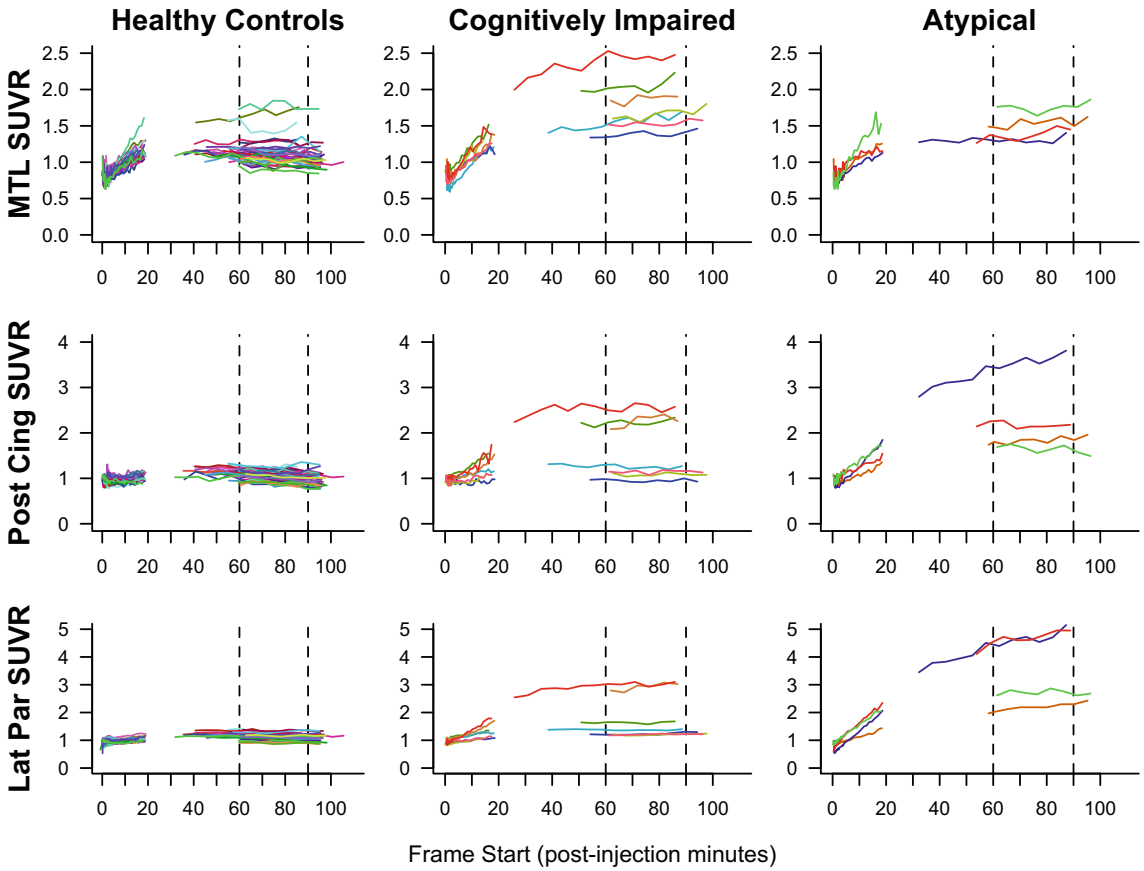

Fig. 2 SUVR by time. SUVRs are shown for the MTL (top row), posterior cingulate cortex (middle row), and lateral parietal cortex (bottom row). SUVR = Standardized Uptake Value Ratio; MTL = Medial Temporal Lobe; Post Cing = Posterior Cingulate Cortex; Lat Par = Lateral Parietal Cortex

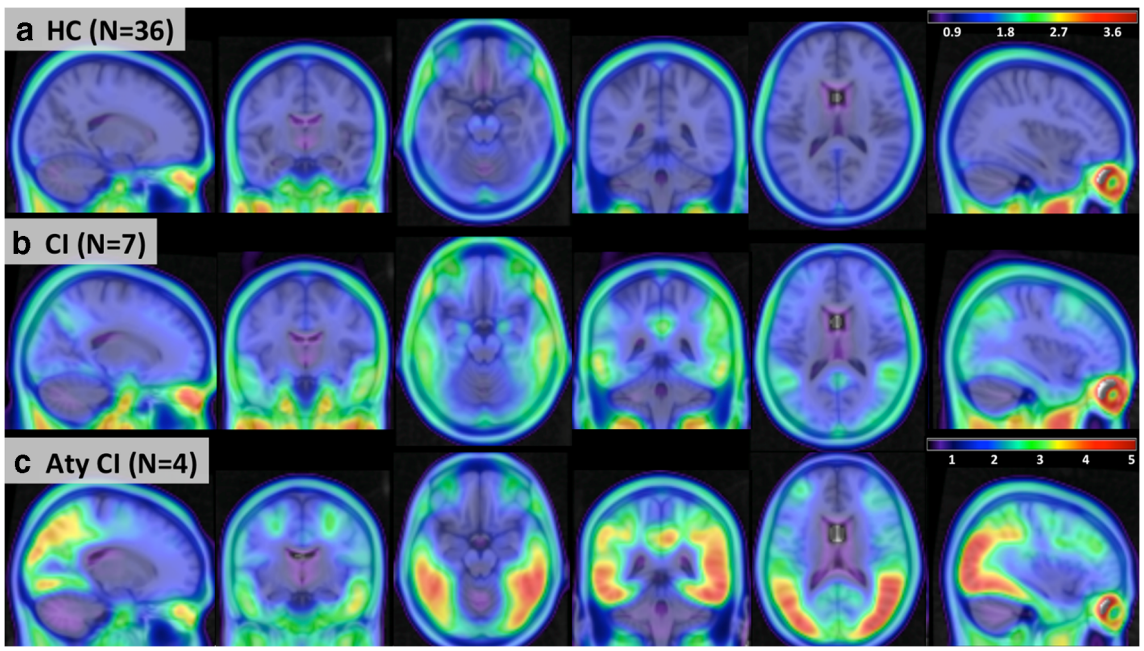

Fig. 3 Average uptake patterns. Group-level SUVR voxelwise averages for 60 to 90 min post-injection are shown for (A) HC, (B) CI, and (C) the atypical CI group. SUVR = Standardized Uptake Value Ratio; HC = Healthy Control; CI = Cognitive Impairment; Aty CI = Atypical Cognitive Impairment

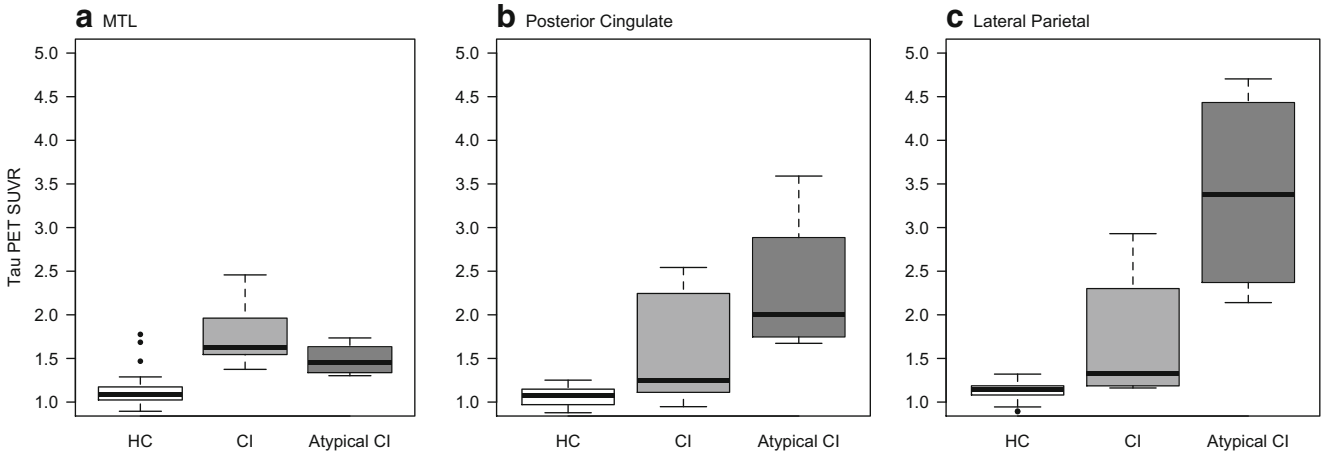

Fig. 4 Regional uptake. Mean regional ^{18}F-PI-2620 SUVR values corresponding to 60 to 90 min post-injection for the MTL (A), posterior cingulate (B), and lateral parietal (C). SUVR = Standardized Uptake Value Ratio; MTL = Medial Temporal Lobe; HC = Healthy Control; CI = Cognitive Impairment; Atypical CI = Atypical Cognitive Impairment

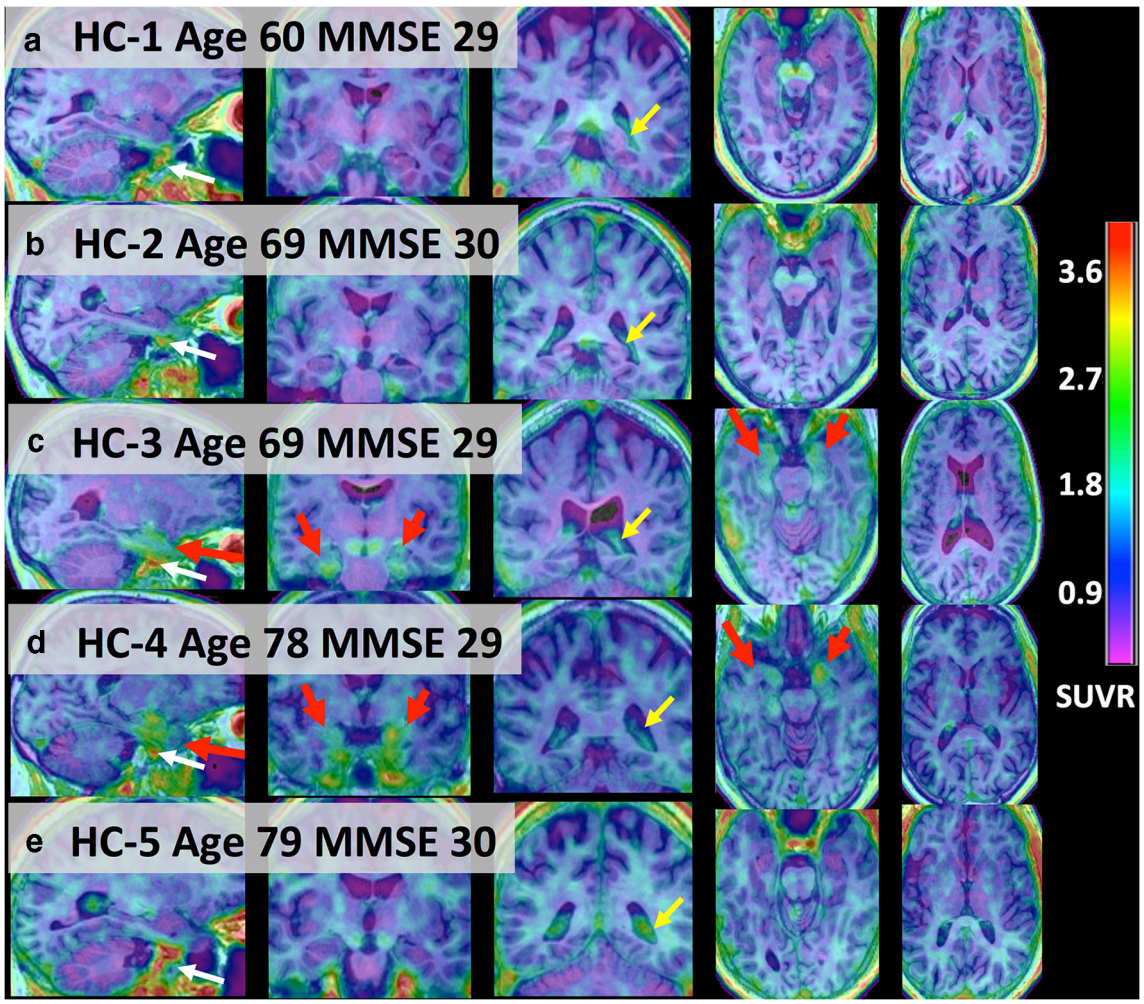

Fig. 5 Voxelwise data for individual HCs. One participant is shown per row. Focally elevated tau PET is observed in HC3 and HC4 (red arrows). Low-level off-target binding is seen in the choroid plexus (yellow arrows), and higher levels of off-target binding are seen in venous sinuses (the cavernous sinus region is indicated with white arrows). Regions in the basal ganglia show consistently low signal across participants. HC = Healthy Control; MMSE = Mini-Mental State Examination; SUVR = Standardized Uptake Value Ratio

substantia nigra, venous sinuses, and choroid plexus (Fig. 5(C, D)). Individuals among the typical CI group showed consistent involvement in the MTL and variable levels of cortical uptake across participants (Fig. 6). Levels of cortical involvement generally tracked with disease severity, with severe cases showing more extensive cortical uptake (Fig. 6(A)) and mild cases showing signal that was restricted to the MTL (Fig. 6(B)). The atypical CI group showed robust elevations throughout posterior association cortices with relative sparing of the medial temporal lobe and frontal cortices across all individual atypical patients (Fig. 7).

Semantic variant primary progressive aphasia

Focal uptake was observed in the anterior temporal pole for one of two patients with svPPA. The younger svPPA patient did not show evidence of elevations that colocalized with atrophy in the anterior temporal lobe (Fig. 8(A)). However, the older svPPA

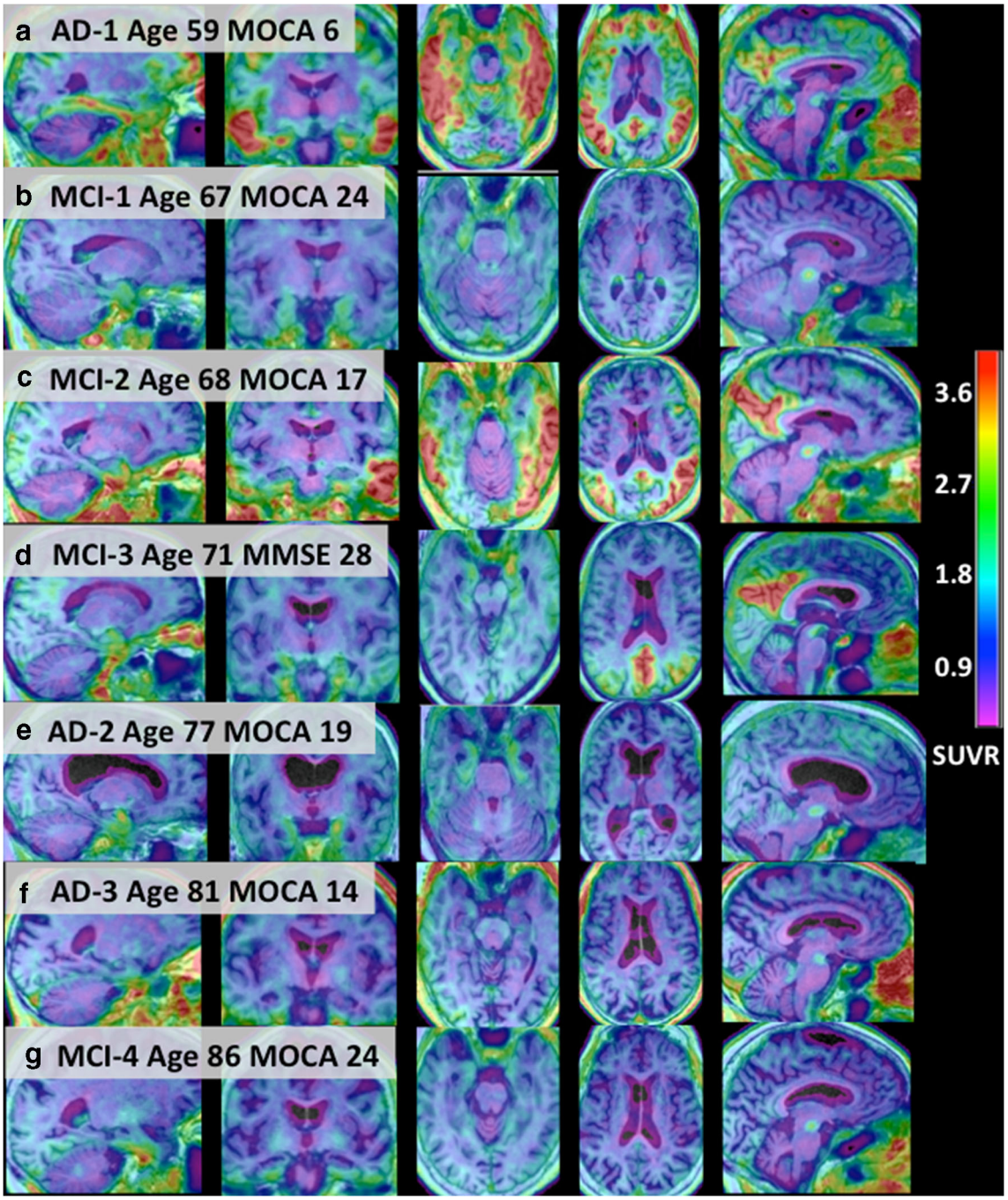

Fig. 6 Voxelwise data for individual CI participants. One participant is shown per row. CI = Cognitive Impairment; MCI = Mild Cognitive Impairment; AD = Alzheimer's Disease; MOCA = Montreal Cognitive Assessment; SUVR = Standardized Uptake Value Ratio

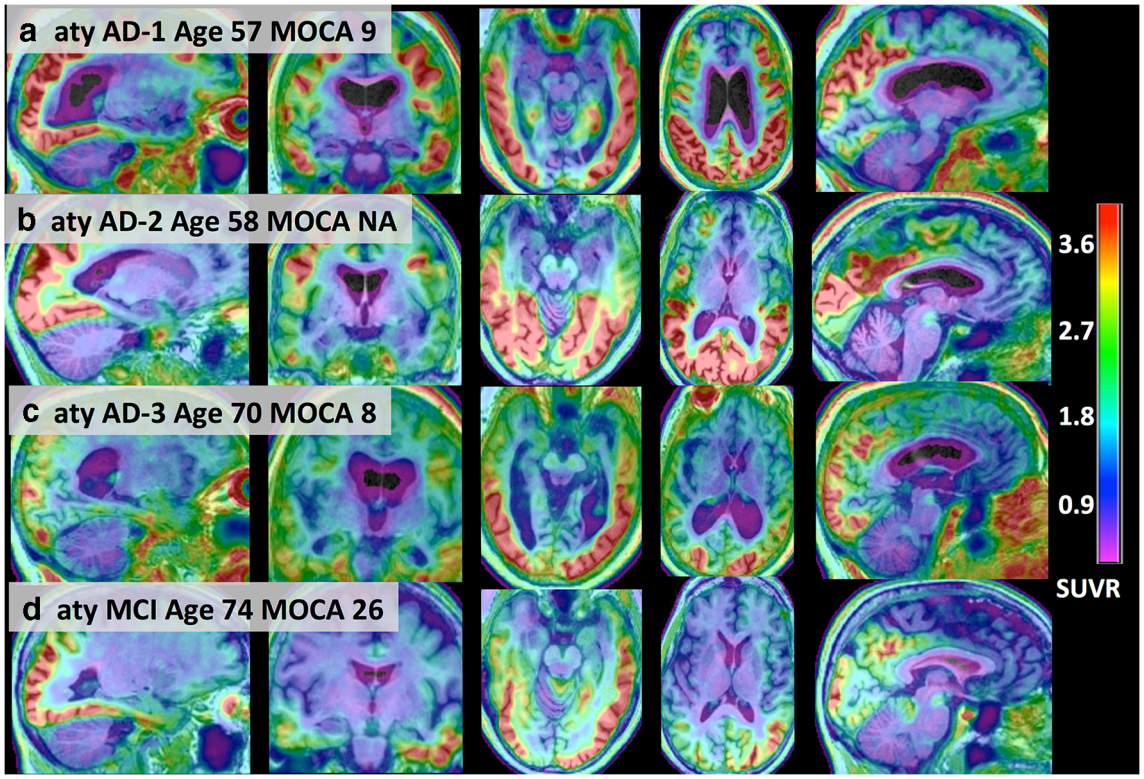

Fig. 7 Voxelwise data for individual atypical CI participants. One participant per row. aty AD = Atypical Alzheimer's Disease; aty MCI = Atypical Mild Cognitive Impairment; MOCA = Montreal Cognitive Assessment; SUVR = Standardized Uptake Value Ratio

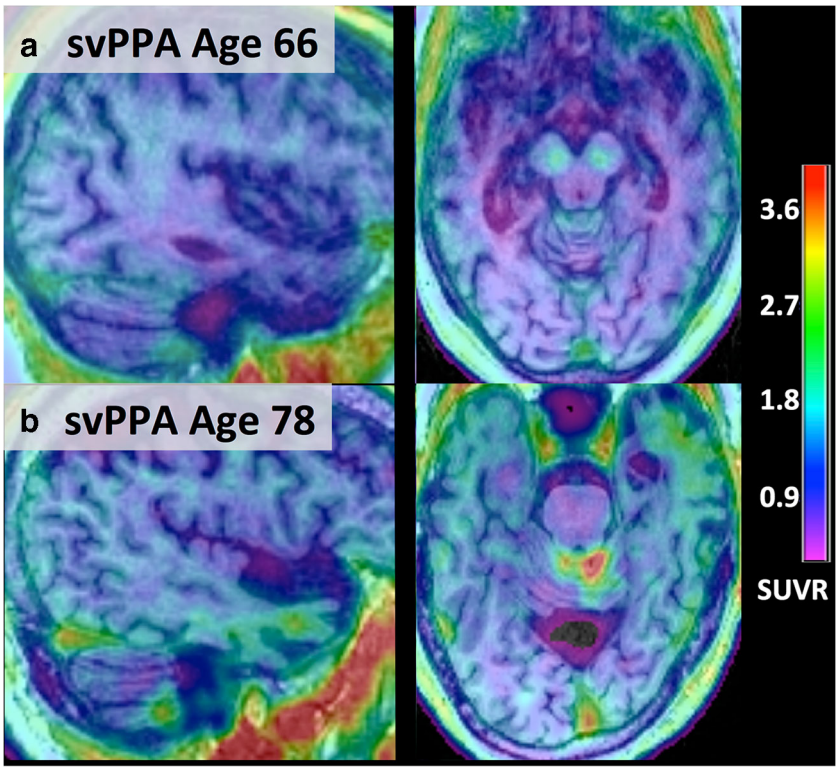

Fig. 8 Individual svPPA participants. One participant is shown per row for (A) a 66-year-old and (B) a 78-year-old participant with svPPA. svPPA = Semantic Variant Primary Progressive Aphasia; SUVR = Standardized Uptake Value Ratio

case did show slightly elevated uptake spanning the lateral and anterior temporal lobe (Fig. 8(B)). In general, this off-target binding was associated with SUVR values less than 2.

Discussion

Overall, we found elevated tau PET signal using ^{18}F-PI-2620 in the context of AD. Specifically, signal in the MTL and posterior cortical association areas were elevated in typical Aβ+amnestic MCI and AD dementia, as well as in atypical non-amnestic clinical presentations of AD. Examination across individual participants showed prominent heterogeneity throughout cortex within amnestic presentations of AD that tended to track with disease severity, whereas elevated signal in the MTL was more consistently present in this group. We found some evidence for slightly elevated values in the temporal lobe of svPPA, suggesting some low-level contributions of off-target binding for ^{18}F-PI-2620. SUVRs normalized to the inferior cerebellum were generally stable 60 to 90 min post-injection, but continued to increase in very high binders (with SUVRs > 3). This work is the first to report the pattern and magnitude of ^{18}F-PI-2620 tau PET across a broad spectrum of ages and clinical diagnoses, and highlights the promise of this novel second-generation tau PET ligand to measure tau aggregates throughout the course of AD.

There is an urgent need to develop and study disease-specific markers in AD. In recent years, rapid development has been made on in vivo measurements of Aβ and tau imaging markers, with increasing applications present in the research setting. This movement in the field is reflected in the recent National Institute of Aging-Alzheimer's Association (NIA-AA) research criteria for AD, which promotes a biological definition of the disease by categorizing individuals across **A**myloid, **T**au, and **N**eurodegenerative dimensions ("A-T-N") [23]. Although Aβ PET measures have been available for over a decade [24], tau PET ligands have only recently been integrated with multiple different PET ligands currently under investigation [25]. The ability to measure tau aggregation accurately holds particular promise as a biomarker for AD, given that tau deposits are known to be more proximal to clinical deficits as compared with Aβ plaques [10], and the majority of Aβ-induced toxicity is thought to be mediated by tau accumulation [11]. Further, the field has seen a string of failures in clinical trials of anti-Aβ approaches [26, 27], and there is some hope that targeting tau may be a more effective strategy [28]. Given that the amount and pattern of tau pathology vary across patients diagnosed clinically with Alzheimer's disease dementia [5], the ability to screen for the presence of Aβ and tau pathology would also assist in the design and enrollment of clinical trials. Thus, although the incorporation of tau PET into the research setting is a recent advancement, there is strong agreement in the field of the importance of this modality for in vivo assessment of tau in humans.

Promising tau PET ligands have been available for over 5 years, including ^{18}F-AV1451 [2], ^{18}F-GTP1 [29], ^{18}F-RO6958948 [30], and more recently ^{18}F-MK6240 [31] as well as ^{18}F-PI-2620 [12, 13]. Initial work examining tau PET has provided important insights and is largely consistent with expected patterns of tangle deposition established in postmortem studies [32, 33] and large group-level differences between healthy controls and patients with AD [4, 5, 34], as well as early focal signal in older, Aβ-positive HC ("preclinical AD") that is associated with subtle memory changes [6, 35]. However, there is evidence of off-target binding that may contaminate relevant signal in target regions. For instance, ^{18}F-AV1451, which is the most extensively studied ligand to date, demonstrates off-target binding in the choroid plexus, which is adjacent to the hippocampus and therefore compromises the ability to measure tau uptake in this key AD region [36]. Off-target binding has also been observed in the basal ganglia, which may imply off-target binding to iron accumulation or possibly focal neuronal injury such as small infarcts and white matter disease [36, 37]. It remains unclear whether these sources of off-target binding will impact the ability to use tau PET as a diagnostic tool in certain situations. Given these uncertainties, it is important for the field to apply novel tau ligands and evaluate their utility as they become available.

To this end, we explored ^{18}F-PI-2620 PET across a broad range of ages and clinical presentations. This work builds off recent work exploring ^{18}F-PI-2620 in 10 healthy controls and 12 AD patients [12, 13]. However, this work was limited by a younger age in the healthy control group (mean age of 59 years compared with 69 years in the AD group), which may exaggerate diagnostic differences and minimize off-target binding. Specifically, our dataset of forty-nine participants spanned older healthy controls between age 61 and 86, Aβ+MCI, and Aβ+ patients with clinical AD dementia, as well as svPPA. Given multiple reports showing differences in tau PET magnitude between typical and atypical AD [9, 32], we additionally separated our patients with clinical impairment into typical amnestic and atypical non-amnestic groups based on these clinical features. Overall, we found elevations in ^{18}F-PI-2620 Tau PET across the spectrum of AD in regions known to be impacted in AD (medial temporal lobe, posterior cingulate, and lateral parietal). Specifically, we found group differences between healthy controls and clinically impaired groups (Aβ+MCI and Aβ+AD dementia). When examining the clinically impaired group, we found a more robust posterior signal in atypical AD patients that presented clinically with features of posterior cortical atrophy. Our typical amnestic MCI and AD patients showed heterogeneity in the cortex, with some individuals showing clear tau PET signal in multiple association cortices and some patients showing little signal beyond the MTL. Given our small sample of patients with clinical impairment, we were not able to examine the primary drivers of this heterogeneity. However, previous tau PET studies have shown that tau PET signal may be reduced in older

versus younger participants [5, 32, 34], perhaps due to contributions of various age-related etiologies that are common in older patients and may be drivers of clinical impairment (such as vascular insults, and TDP-43 pathology) [38]. It is also likely that variation in tau PET varies across disease severity [4, 5], as we did tend to see that less-impaired patients showed restricted signal when examining individual participants. Off-target binding was observed in the retina, substantia nigra, and venous sinuses across most participants. Low levels of choroid plexus off-target binding were noticed across some participants. The basal ganglia did not show any evidence of off-target binding, which is a common site of off-target binding across other tracers [36]. Larger datasets with ^{18}F-PI-2620 PET will be needed to understand the factors that best predict the extent of uptake among Aβ+MCI and AD participants in target regions, as well as the prevalence and magnitude of off-target binding.

Examination of two cases with svPPA provided evidence of subtle off-target binding in the anterior temporal lobe in one case. This uptake suggests binding related to degeneration independent of tau aggregations, given that svPPA is most likely associated with TDP-43 pathology [39]. The pattern of focal subtle uptake in patients with TDP-43 has been reported in previous studies with ^{18}F-AV1451 [16, 40, 41]. In the absence of a head-to-head comparison, it is not possible to determine whether the magnitude of this specific source of off-target binding varies across PET ligands.

Overall, our study is the first to comprehensively examine ^{18}F-PI-2620 across a broad spectrum of aging and individuals on the AD spectrum. Our results highlight the utility of this tracer in detecting tau aggregates in AD. Larger studies will be necessary to determine whether the sources of off-target binding will impair the ability of ^{18}F-PI-2620 to measure tau pathology throughout the course of disease, especially regarding longitudinal estimates of change and the ability to detect early signal within the medial temporal lobe that is expected to emerge among healthy older adults. Additionally, further work is needed to explore potential reference regions as well as the optimal time acquisition period for data acquisition.

Acknowledgments The authors acknowledge Life Molecular Imaging for providing the precursor for this study.

Funding information This study was funded by the NIH (K01-AG051718 and R21-AG058859, Mormino; R01-AG048076, Wagner; P50-AG047366, Henderson; R01-AG061120, Zeineh), General Electric (GE), the Stanford Wu Tsai Neuroscience Institute, and the Stanford Precision Health and Integrated Diagnostics Center.

Compliance with ethical standards

Conflict of interest Author Elizabeth Mormino receives research funds from the National Institutes of Health grants K01-AG051718 and R21-AG058859. Dr. Mormino has been a consultant for Eli Lilly, Biogen Idec, F Hoffmann-La Roche Ltd., Janssen, and Alector.

Author Michael Zeineh receives research funds from the National Institutes of Health grant R01-AG061120 and from General Electric (GE).

Michelle James reports travel compensation from World Molecular Imaging Congress (WMIC) to present on Emerging neuroimaging techniques and present at an educational session on "best practices for small animal PET imaging."

Author Sharon Sha receives research support from Biogen Idec, F Hoffmann-La Roche Ltd., Genentech, and Novartis for her role as Investigator in Clinical Trials. Dr. Sha has been a consultant for Abelson Taylor, Baird, Clearview Healthcare Partners, SelfCare Catalysts Inc., and the University of Southern California. Dr. Sha is funded by National Institutes of Health grants P50 AG047366 (Stanford Alzheimer's Disease Center) and R01 AG048076.

Author Greg Zaharchuk has received research support from GE Healthcare, LifeMI, Stanford AI Laboratory (SAIL), and the National Institutes of Health grants P50 AG047366. Dr. Zaharchuk has equity in Subtle Medical.

Author Anthony Wagner receives research funds from the National Institutes of Health grant R01-AG048076.

All other authors declare that he/she has no conflict of interest.

Ethical approval All procedures performed in studies involving human participants were in accordance with the ethical standards of the institutional and/or national research committee and with the 1964 Helsinki declaration and its later amendments or comparable ethical standards.

Informed consent Informed consent was obtained from all individual participants included in the study.

References

1. Montine TJ, Phelps CH, Beach TG, Bigio EH, Cairns NJ, Dickson DW, et al. National Institute on Aging-Alzheimer's Association guidelines for the neuropathologic assessment of Alzheimer's disease: a practical approach. Acta Neuropathol. 2012;123:1–11. https://doi.org/10.1007/s00401-011-0910-3.
2. Chien DT, Bahri S, Szardenings AK, Walsh JC, Mu F, Su MY, et al. Early clinical PET imaging results with the novel PHF-tau radioligand [F-18]-T807. J Alzheimers Dis. 2013;34:457–68. https://doi.org/10.3233/JAD-122059.
3. Fleisher AS, Pontecorvo MJ, Devous MD Sr, Lu M, Arora AK, Truocchio SP, et al. Positron emission tomography imaging with [18F]flortaucipir and postmortem assessment of Alzheimer disease neuropathologic changes. JAMA Neurol. 2020. https://doi.org/10.1001/jamaneurol.2020.0528.
4. Johnson KA, Schultz A, Betensky RA, Becker JA, Sepulcre J, Rentz D, et al. Tau positron emission tomographic imaging in aging and early Alzheimer disease. Ann Neurol. 2016;79:110–9. https://doi.org/10.1002/ana.24546.
5. Pontecorvo MJ, Devous MD Sr, Navitsky M, Lu M, Salloway S, Schaerf FW, et al. Relationships between flortaucipir PET tau binding and amyloid burden, clinical diagnosis, age and cognition. Brain. 2017;140:748–63. https://doi.org/10.1093/brain/aww334.
6. Sperling RA, Mormino EC, Schultz AP, Betensky RA, Papp KV, Amariglio RE, et al. The impact of amyloid-beta and tau on prospective cognitive decline in older individuals. Ann Neurol. 2019;85:181–93. https://doi.org/10.1002/ana.25395.
7. Jack CR Jr, Wiste HJ, Therneau TM, Weigand SD, Knopman DS, Mielke MM, et al. Associations of amyloid, tau, and neurodegeneration biomarker profiles with rates of memory decline among individuals without dementia. JAMA. 2019;321:2316–25. https://doi.org/10.1001/jama.2019.7437.

8. Scholl M, Lockhart SN, Schonhaut DR, O'Neil JP, Janabi M, Ossenkoppele R, et al. PET imaging of tau deposition in the aging human brain. Neuron. 2016;89:971–82. https://doi.org/10.1016/j.neuron.2016.01.028.
9. Ossenkoppele R, Schonhaut DR, Scholl M, Lockhart SN, Ayakta N, Baker SL, et al. Tau PET patterns mirror clinical and neuroanatomical variability in Alzheimer's disease. Brain. 2016;139:1551–67. https://doi.org/10.1093/brain/aww027.
10. Nelson PT, Braak H, Markesbery WR. Neuropathology and cognitive impairment in Alzheimer disease: a complex but coherent relationship. J Neuropathol Exp Neurol. 2009;68:1–14. https://doi.org/10.1097/NEN.0b013e3181919a48.
11. Bennett DA, Schneider JA, Wilson RS, Bienias JL, Arnold SE. Neurofibrillary tangles mediate the association of amyloid load with clinical Alzheimer disease and level of cognitive function. Arch Neurol. 2004;61:378–84. https://doi.org/10.1001/archneur.61.3.378.
12. Bullich S, Barret O, Constantinescu C, Sandiego C, Mueller A, Berndt M, et al. Evaluation of dosimetry, quantitative methods and test-retest variability of (18)F-PI-2620 PET for the assessment of tau deposits in the human brain. J Nucl Med. 2019. https://doi.org/10.2967/jnumed.119.236240.
13. Kroth H, Oden F, Molette J, Schieferstein H, Capotosti F, Mueller A, et al. Discovery and preclinical characterization of [(18)F]PI-2620, a next-generation tau PET tracer for the assessment of tau pathology in Alzheimer's disease and other tauopathies. Eur J Nucl Med Mol Imaging. 2019;46:2178–89. https://doi.org/10.1007/s00259-019-04397-2.
14. Beyer L, Nitschmann A, Barthel H, van Eimeren T, Unterrainer M, Sauerbeck J, et al. Early-phase [(18)F]PI-2620 tau-PET imaging as a surrogate marker of neuronal injury. Eur J Nucl Med Mol Imaging. 2020. https://doi.org/10.1007/s00259-020-04788-w.
15. Mueller A, Bullich S, Barret O, Madonia J, Berndt M, Papin C, et al. Tau PET imaging with (18)F-PI-2620 in patients with Alzheimer's disease and healthy controls: a first-in-human study. J Nucl Med. 2019. https://doi.org/10.2967/jnumed.119.236224.
16. Sousa JM, Appel L, Engstrom M, Papadimitriou S, Nyholm D, Larsson EM, et al. Evaluation of zero-echo-time attenuation correction for integrated PET/MR brain imaging-comparison to head atlas and (68)Ge-transmission-based attenuation correction. EJNMMI Phys. 2018;5:20. https://doi.org/10.1186/s40658-018-0220-0.
17. Vemuri P, Lowe VJ, Knopman DS, Senjem ML, Kemp BJ, Schwarz CG, et al. Tau-PET uptake: regional variation in average SUVR and impact of amyloid deposition. Alzheimers Dement (Amst). 2017;6:21–30. https://doi.org/10.1016/j.dadm.2016.12.010.
18. Grabner G, Janke AL, Budge MM, Smith D, Pruessner J, Collins DL. Symmetric atlasing and model based segmentation: an application to the hippocampus in older adults. Med Image Comput Comput Assist Interv. 2006;9:58–66. https://doi.org/10.1007/11866763_8.
19. Fischl B. FreeSurfer Neuroimage. 2012;62:774–81. https://doi.org/10.1016/j.neuroimage.2012.01.021.
20. Fischl B, Salat DH, Busa E, Albert M, Dieterich M, Haselgrove C, et al. Whole brain segmentation: automated labeling of neuroanatomical structures in the human brain. Neuron. 2002;33:341–55. https://doi.org/10.1016/s0896-6273(02)00569-x.
21. Desikan RS, Segonne F, Fischl B, Quinn BT, Dickerson BC, Blacker D, et al. An automated labeling system for subdividing the human cerebral cortex on MRI scans into gyral based regions of interest. Neuroimage. 2006;31:968–80. https://doi.org/10.1016/j.neuroimage.2006.01.021.
22. Tang-Wai DF, Graff-Radford NR, Boeve BF, Dickson DW, Parisi JE, Crook R, et al. Clinical, genetic, and neuropathologic characteristics of posterior cortical atrophy. Neurology. 2004;63:1168–74. https://doi.org/10.1212/01.wnl.0000140289.18472.15.
23. Jack CR Jr, Bennett DA, Blennow K, Carrillo MC, Dunn B, Haeberlein SB, et al. NIA-AA research framework: toward a biological definition of Alzheimer's disease. Alzheimers Dement. 2018;14:535–62. https://doi.org/10.1016/j.jalz.2018.02.018.
24. Klunk WE, Engler H, Nordberg A, Wang Y, Blomqvist G, Holt DP, et al. Imaging brain amyloid in Alzheimer's disease with Pittsburgh compound-B. Ann Neurol. 2004;55:306–19. https://doi.org/10.1002/ana.20009.
25. Scholl M, Maass A, Mattsson N, Ashton NJ, Blennow K, Zetterberg H, et al. Biomarkers for tau pathology. Mol Cell Neurosci. 2019;97:18–33. https://doi.org/10.1016/j.mcn.2018.12.001.
26. Egan MF, Kost J, Voss T, Mukai Y, Aisen PS, Cummings JL, et al. Randomized trial of verubecestat for prodromal Alzheimer's disease. N Engl J Med. 2019;380:1408–20. https://doi.org/10.1056/NEJMoa1812840.
27. Ostrowitzki S, Lasser RA, Dorflinger E, Scheltens P, Barkhof F, Nikolcheva T, et al. A phase III randomized trial of gantenerumab in prodromal Alzheimer's disease. Alzheimers Res Ther. 2017;9:95. https://doi.org/10.1186/s13195-017-0318-y.
28. Giacobini E, Gold G. Alzheimer disease therapy–moving from amyloid-beta to tau. Nat Rev Neurol. 2013;9:677–86. https://doi.org/10.1038/nrneurol.2013.223.
29. Teng E, Ward M, Manser PT, Sanabria-Bohorquez S, Ray RD, Wildsmith KR, et al. Cross-sectional associations between [(18)F]GTP1 tau PET and cognition in Alzheimer's disease. Neurobiol Aging. 2019;81:138–45. https://doi.org/10.1016/j.neurobiolaging.2019.05.026.
30. Kuwabara H, Comley RA, Borroni E, Honer M, Kitmiller K, Roberts J, et al. Evaluation of (18)F-RO-948 PET for quantitative assessment of tau accumulation in the human brain. J Nucl Med. 2018;59:1877–84. https://doi.org/10.2967/jnumed.118.214437.
31. Betthauser TJ, Cody KA, Zammit MD, Murali D, Converse AK, Barnhart TE, et al. In vivo characterization and quantification of neurofibrillary tau PET radioligand (18)F-MK-6240 in humans from Alzheimer disease dementia to young controls. J Nucl Med. 2019;60:93–9. https://doi.org/10.2967/jnumed.118.209650.
32. Scholl M, Ossenkoppele R, Strandberg O, Palmqvist S, Swedish Bio FS, Jogi J, et al. Distinct 18F-AV-1451 tau PET retention patterns in early- and late-onset Alzheimer's disease. Brain. 2017;140:2286–94. https://doi.org/10.1093/brain/awx171.
33. Braak H, Braak E. Neuropathological stageing of Alzheimer-related changes. Acta Neuropathol. 1991;82:239–59.
34. Jack CR Jr, Wiste HJ, Schwarz CG, Lowe VJ, Senjem ML, Vemuri P, et al. Longitudinal tau PET in ageing and Alzheimer's disease. Brain. 2018;141:1517–28. https://doi.org/10.1093/brain/awy059.
35. Maass A, Lockhart SN, Harrison TM, Bell RK, Mellinger T, Swinnerton K, et al. Entorhinal tau pathology, episodic memory decline, and neurodegeneration in aging. J Neurosci. 2018;38:530–43. https://doi.org/10.1523/JNEUROSCI.2028-17.2017.
36. Lowe VJ, Curran G, Fang P, Liesinger AM, Josephs KA, Parisi JE, et al. An autoradiographic evaluation of AV-1451 tau PET in dementia. Acta Neuropathol Commun. 2016;4:58. https://doi.org/10.1186/s40478-016-0315-6.
37. Lockhart SN, Ayakta N, Winer JR, La Joie R, Rabinovici GD, Jagust WJ. Elevated 18F-AV-1451 PET tracer uptake detected in incidental imaging findings. Neurology. 2017;88:1095–7. https://doi.org/10.1212/WNL.0000000000003724.
38. Pierce AL, Kawas CH. Dementia in the oldest old: beyond Alzheimer disease. PLoS Med. 2017;14:e1002263. https://doi.org/10.1371/journal.pmed.1002263.
39. Bergeron D, Gorno-Tempini ML, Rabinovici GD, Santos-Santos MA, Seeley W, Miller BL, et al. Prevalence of amyloid-beta pathology in distinct variants of primary progressive aphasia. Ann Neurol. 2018;84:729–40. https://doi.org/10.1002/ana.25333.
40. Smith R, Santillo AF, Waldo ML, Strandberg O, Berron D, Vestberg S, et al. (18)F-Flortaucipir in TDP-43 associated

frontotemporal dementia. Sci Rep. 2019;9:6082. https://doi.org/10.1038/s41598-019-42625-9.

41. Schaeverbeke J, Celen S, Cornelis J, Ronisz A, Serdons K, Van Laere K, et al. Binding of [(18)F]AV1451 in post mortem brain slices of semantic variant primary progressive aphasia patients. Eur J Nucl Med Mol Imaging. 2019. https://doi.org/10.1007/s00259-019-04631-x.